Appl Phys B (2011) 102: 615–619
DOI 10.1007/s00340-010-4244-y

Applied Physics B
Lasers and Optics

Wave guiding properties and sensitivity of D-shaped optical fiber microwire devices

J.-l. Kou · Z.-d. Huang · G. Zhu · F. Xu · Y.-q. Lu

Received: 1 May 2010 / Revised version: 1 August 2010 / Published online: 16 October 2010

Abstract D-shaped optical fiber microwire (OFM) devices are investigated theoretically. They can be obtained by wrapping OFMs on removable rods or laying the OFMs on disposable substrates. Optical wave guiding properties of these devices are discussed with numerical simulations. Dispersion properties of OFMs with different radii are studied as well. A grating-based D-shaped OFM is proposed for sensing applications. The corresponding sensitivity could reach 1100 nm/RIU (refractive index unit) due to its large outside evanescent field.

1 Introduction

Conventional D-shaped fibers are fabricated by drawing a flat-side preform [1] or polishing standard cylindrical optical fibers laterally [2, 3]. The evanescent field of the propagating light wave in a D-shaped fiber is accessible through the removed section of the cladding, which gives rise to many interesting applications such as fiber polarizers, spectral filters, optical sensors and optical interconnects. Because of the mode compatibility with standard fibers, D-shaped fibers may have low splice loss. However, their core diameters of around ten micrometers limit the evanescent field and minimum bending radius. Due to the relatively large core diameter, only a small portion of the total optical power flows outside the core. In addition, it is not convenient to manufacture compact devices with normal D-shaped fibers because they are easily broken when bent. The high bending loss is also a possible issue. Following a fast development of fabrication technology, a subwavelength-diameter optical fiber microwire (OFM) in recent years [4, 5] has emerged as an ideal element of microfiber devices because of low cost, low loss and very large evanescent fields [6–12]. A lot of different OFM devices have been proposed and demonstrated, mainly in the form of resonators. It is also possible to fabricate new devices keeping the conventional D-shape but with much thinner core (hundreds of nanometers), larger evanescent field and more compact size.

In this paper, we propose fabrication techniques of D-shaped OFM devices. Their wave guiding properties are studied including light intensity distribution and chromatic dispersion. A grating-based D-shaped OFM device is proposed for sensing applications. The corresponding sensitivity could reach a very high level due to its large evanescent field.

2 Schematic of D-shaped OFM device

A D-shaped OFM device can be fabricated by coating an OFM on a removable substrate or wrapping it on a removable rod, as shown in Fig. 1. First, a standard single-mode fiber is pulled using the mature flame-brushing technique [8, 13]. An OFM with much smaller diameter is thus obtained. The dimension of the microwire could be well controlled by adjusting the flame movement and the fiber stretching rate. Second, the OFM can be laid on a flat removable substrate (for example, polymethylmethacrylate—PMMA) and surrounded by a low-loss, low-index polymer (for example, UV375 or Teflon). The schematic diagram is

J.-l. Kou · Z.-d. Huang · G. Zhu · F. Xu (✉) · Y.-q. Lu
Department of Materials Science and Engineering, College of Engineering and Applied Sciences and National Laboratory of Solid State Microstructures, Nanjing University, Nanjing 210093, P.R. China
e-mail: feixu@nju.edu.cn
Fax: +86-053-83686053

Y.-q. Lu
e-mail: yqlu@nju.edu.cn

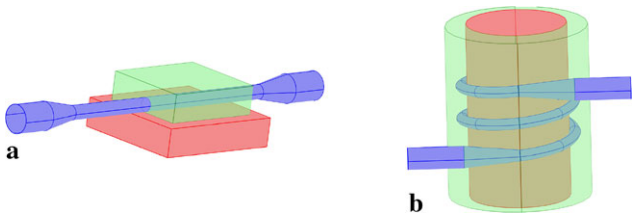

Fig. 1 Schematic diagram of D-shaped OFM devices. (**a**) OFM laid on a substrate; the blue, light green and red parts refer to OFM, coating and substrate, respectively. (**b**) OFM wrapped around a rod to form coils; the *blue*, *light green* and *red parts* represent OFM, coating and rod, respectively

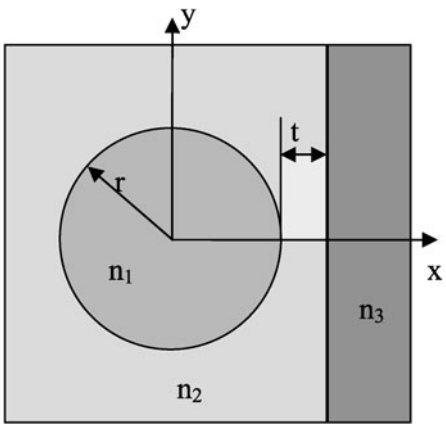

Fig. 2 Schematic cross-sectional diagram of a D-shaped OFM device; n_1, n_2 and n_3 are the refractive indices of the OFM, the coating and the environment, respectively; t is the distance between the OFM and the outside environment; r is the OFM radius

shown in Fig. 1a. After the substrate is removed, the structure is similar to a conventional D-shaped fiber as it also has a flat side wall close to the core. We call it a straight D-shaped OFM device (type I). The OFM also can be wrapped around a removable rod (red part in Fig. 2b) and coated by low-index polymer; then another kind of 'D-shaped' OFM device (type II) is obtained by getting rid of the rod. It has a natural inner fluid or gas channel with large evanescent field inside. Type-II devices could be very compact by wrapping multi-turn OFMs on the rod with the diameter of hundreds of micrometers, similar to a 3D microfiber resonator sensor and a micrograting on a microstructured rod. Both type I and type II may have large evanescent field outside of the flat top or inside the channel, owing to the OFM's small diameter (hundreds of nanometers to several micrometers). Being fabricated from standard single-mode fibers, the input/output parts are still original ones so these new D-shaped OFM devices do not experience any connecting difficulties in a sensing or communication link. They are very flexible to realize different functions by pre-processing the substrate or rod. For example, a micrograting can be realized if the substrate has a surface corrugation structure or the rod is a microstructured rod with some air holes arranged in a circle. If the substrate or the rod is coated with a metal film, even surface plasmon polaritons can be excited.

3 Simulation model

Both type I and type II have a similar cross section, as shown in Fig. 2. We assume that n_1, n_2 and n_3 are the indices of OFM, coating and outside environment, respectively; r is the radius of the OFM; t is the distance between the OFM and the outside medium. Bent dielectric waveguides, especially bent fibers, experience loss, which decreases exponentially with the curvature radius [14]. So, in our work, we assume that the radius of the rod in type II is large enough compared to that of the OFM. The following Sellmeier-type dispersion formula (at room temperature) is employed to deduce the refractive index of the fused-silica OFM at different wavelengths [15]:

$$n^2 - 1 = \frac{0.6965325\lambda^2}{\lambda^2 - (0.0660932)^2} + \frac{0.4083099\lambda^2}{\lambda^2 - (0.1181101)^2} + \frac{0.8968766\lambda^2}{\lambda^2 - (9.8961604)^2}, \quad (1)$$

where the unit of λ is μm.

The effective index n_{eff} is an important and fundamental parameter in many applications. In this work, it is numerically calculated using the finite-element method (FEM) with the commercial software COMSOL 3.4. Figure 3 shows the dependence of n_{eff} of the rigid mode on the OFM radius r, assuming the refractive indices of the OFM, of the embedding low refractive index polymer (Teflon) and of the environment (air) to be $n_1 = 1.4443$, $n_2 = 1.311$ and $n_3 = 1$, at a wavelength of 1550 nm, respectively. While t is set at 10 nm and 1000 nm, three wavelengths are chosen: $\lambda = 632.8$ nm, 980 nm and 1550 nm. We only consider the fundamental rigid mode which has the largest propagation constant. It is the only mode that is well confined in the vicinity of the OFM [2]. Generally, n_{eff} increases with larger r in both type I and type II because less fraction of the mode is propagating in air. Of course, n_{eff} also changes with t; here we did not give the results for different t because it changes very slowly as can be deduced from Fig. 3.

4 The power fraction carried by the OFM

In practical applications such as evanescent wave based optical sensing, it is important to know the profile of the light intensity distribution around the waveguide. In the case of D-shaped OFM devices, we only consider the time-averaged power flow along the z-direction, which is the axis of the

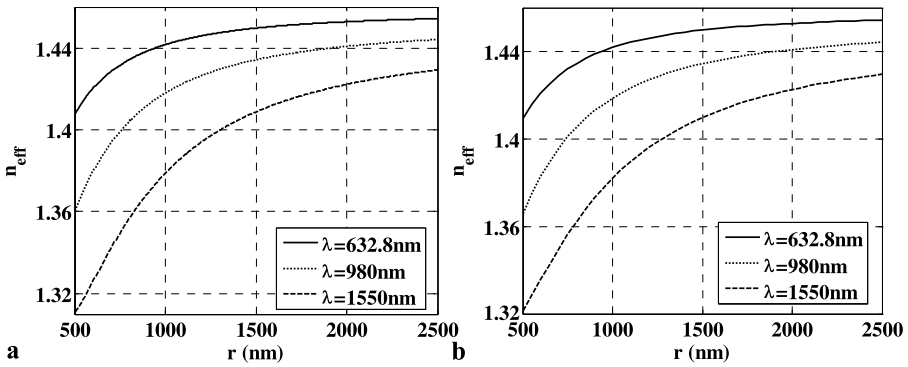

Fig. 3 Effective index as a function of the radius of the OFM (r) at different wavelengths with (**a**) $t = 10$ nm, (**b**) $t = 1$ μm

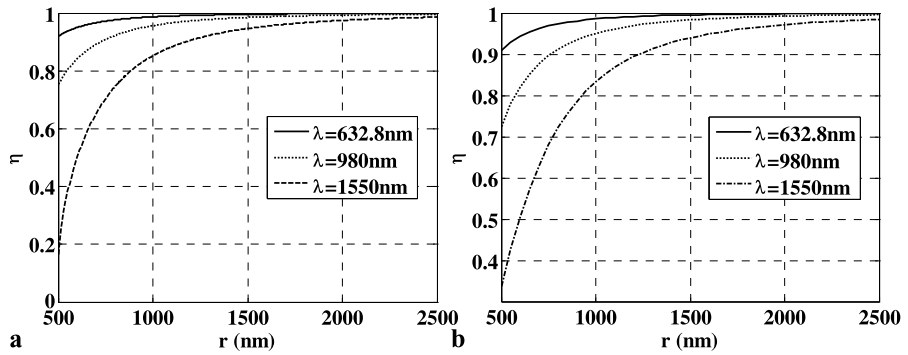

Fig. 4 The power fraction carried within the OFM as a function of its radius (r) at different wavelengths with (**a**) $t = 10$ nm, (**b**) $t = 1$ μm

fiber. The z-component of the Poynting vectors is described as follows [16]:

$$S_z = \frac{1}{2}\,\mathrm{Re}\big[E_x H_y^* - E_y H_x^*\big], \tag{2}$$

where E_x, H_x, E_y and H_y represent the electric and magnetic components of the electromagnetic field along the x- and y-axes, respectively. Then, we obtain the fraction of power inside the OFM, defined as η:

$$\eta = \frac{\int_0^{2\pi}\int_0^{r} S_z u\,\mathrm{d}u\,\mathrm{d}\phi}{\int_0^{2\pi}\int_0^{\infty} S_z u\,\mathrm{d}u\,\mathrm{d}\phi}. \tag{3}$$

η as a function of the radius of the OFM at different wavelengths is shown in Fig. 4, in which the solid, dotted and dashed lines are plotted for $\lambda = 632.8$ nm, 980 nm and 1550 nm, respectively. Generally, η increases when λ decreases or r increases. From Fig. 4, we can easily obtain different fractions of power by controlling r at different wavelengths. When $r < 600$ nm and $\lambda = 1550$ nm, only <50% power is kept inside an OFM.

5 Dispersion

The group-velocity dispersion (GVD) or chromatic dispersion is a primary cause of concern when dealing with short-duration pulse, high bit rate single-mode wavelength division multiplexing (WDM) systems because light from a typical optical source contains different wavelength components which travel at different speeds. Pulses broaden because of dispersion. GVD is described as [17]

$$D = -\frac{1}{2\pi c}\left(\lambda^2\frac{\mathrm{d}^2\beta}{\mathrm{d}^2\lambda} + 2\lambda\frac{\mathrm{d}\beta}{\mathrm{d}\lambda}\right), \tag{4}$$

where β is the propagation constant and ω is the angular frequency of light expressed as $2\pi c/\lambda$ with c the velocity of light in vacuum. Figure 5a and b show D as a function of r at different wavelengths. A very large dispersion (~ -1000 ps km^{-1} nm^{-1}) is obtained at 1550 nm when t approaches zero ($\sim$10 nm in Fig. 5a), which is much larger than that of conventional D-shaped fibers of around several ps km^{-1} nm^{-1}. From the figure, a larger dispersion normally could be obtained with smaller fiber diameter.

As we know, GVD is an important parameter in various fiber-based nonlinear applications, especially in supercontinuum (SC) generation, which could be applied in pulse compressors, parametric amplifiers and WDM telecom sources [18–22]. The mechanisms responsible for SC generation include soliton fission, stimulated Raman scattering, four-wave mixing, self-phase modulation and cross-phase modulation. In standard optical fibers there is only one zero-dispersion wavelength (ZDW) in the optical spectrum, typically at 1300 nm. It is well known that the gain bandwidth for four-wave mixing is widest in the vicinity of the ZDW due to phase-matching conditions, and that solitons in the vicinity of the ZDW can amplify dispersive waves in

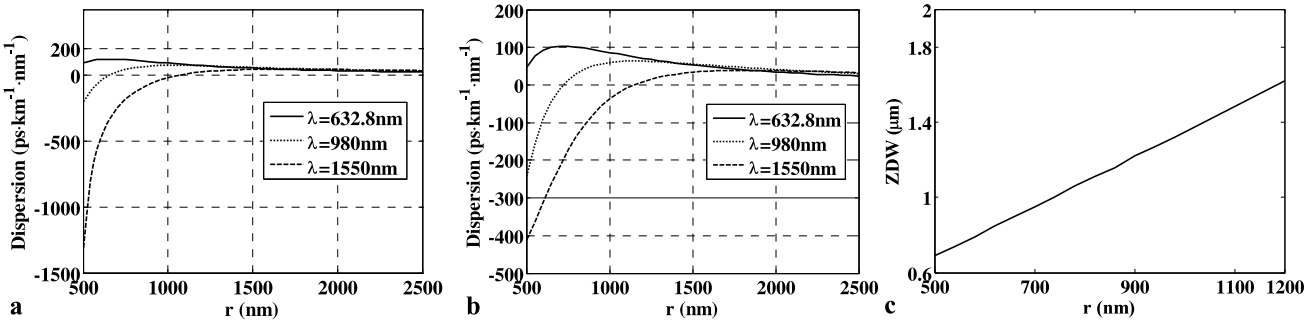

Fig. 5 Dispersion as a function of the radius of an OFM (r) at different wavelengths with (**a**) $t = 10$ nm, (**b**) $t = 1$ μm. (**c**) The ZDW as a function of the radius of an OFM (r) at $\lambda = 1550$ nm with $t = 1$ μm

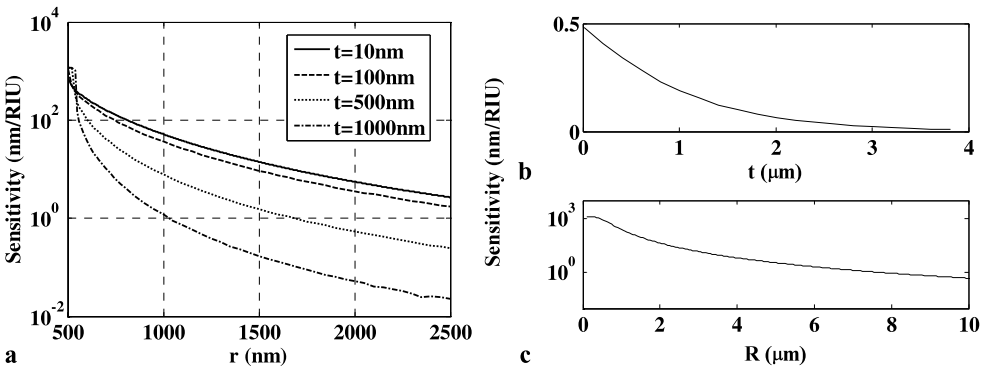

Fig. 6 (**a**) Dependence of the sensitivity on OFM radius (r) for a D-shaped OFM Bragg grating with different values of t at $\lambda = 1550$ nm and $n_3 = 1.33$. (**b**) Dependence of the sensitivity on t for a regular D-shaped fiber based Bragg grating with a typical 9-μm-diameter core. (**c**) Dependence of the sensitivity on its radius R for a directly etched standard FBG without coating

the normal dispersion region (NDR). Supercontinuum generation typically takes place around the ZDW. The ZDWs at different radii of the OFM are shown in Fig. 5b. The ZDW can be designed and realized in the range of 600 nm to 2 μm by choosing a proper OFM radius in the range from 500 nm to 2.5 μm. This would be an advantage to broaden the applications of D-shaped OFM devices in efficient supercontinuum generation and spectral shaping.

6 Refractive-index sensing

Fiber sensors based on fiber Bragg gratings (FBGs) have been potentially developed to measure temperature, pressure or stress due to their many inherent advantages such as wavelength multiplexing and distributed sensing possibilities. But, they are scarcely used to measure the environmental refractive index variation because there is almost no evanescent field penetrating outside of a standard 125-μm-diameter FBG. Although a standard FBG can be etched to remove its cladding and even part of the core, it is easily broken or contaminated without coating. Recently, focused ion beam milling or implantation [23], ultraviolet interference lithography [24] and femtosecond infrared irradiation [25, 26] have been employed to write a FBG on a microfiber for sensing applications. But, these methods are relatively complicated and time consuming. A FBG based on a D-shaped fiber may overcome the drawbacks and has been investigated [27, 28], but the sensitivity is still not high because of its small evanescent field. However, a D-shaped OFM Bragg grating might be a good candidate to increase the sensitivity significantly because of the large outside evanescent field. It can be fabricated in several ways: etching and pulling an FBG; writing into a germanium-doped OFM directly; inducing a surface corrugation on the side flat plane or the removable rod; or wrapping an OFM on a microstructured rod. The sensitivity of all these sensors is determined by the Bragg wavelength shift as a function of the change of refractive index of the analyte when the Bragg condition $\lambda_B = 2n_{eff}\Lambda$ is satisfied [29]:

$$S = \frac{\partial \lambda_B}{\partial n_3} = \frac{\partial \lambda_B}{\partial n_{eff}} \frac{\partial n_{eff}}{\partial n_3} = \frac{\lambda_B}{n_{eff}} \frac{\partial n_{eff}}{\partial n_3}. \quad (5)$$

We assume that $\lambda_B = 1550$ nm and the index of the analyte $n_3 = 1.33$ because most of the refractometric sensors work with aqueous solutions. Figure 6a shows how the sensitivity changes with radius of the OFM. A sensitivity as high as 1100 nm/RIU (refractive index unit) can be achieved when r is reduced to 500 nm, which can be easily obtained using the mature flame brushing technique [8, 13]; however, the sensitivity of a Bragg grating based on a regular D-shaped fiber with a standard 9-μm-diameter core can hardly achieve 1 nm/RIU even at $t = 0$, as shown in Fig. 6b; Fig. 6c shows the dependence of S on the radius R for a directly etched

standard FBG without coating. Although its sensitivity also can reach 1100 nm/RIU if $R < 400$ nm, it is very difficult to get such a thin FBG grating by direct etching. Generally, $S < 100$ nm/RIU is an achievable level for such an etched FBG grating with several micrometers diameter [30]; otherwise, it is too fragile for fabrication and handling.

7 Discussion and conclusions

In this paper, we theoretically investigated D-shaped OFM devices. They can be fabricated by wrapping an OFM on a removable rod or substrate. This kind of device is stable, compact and flexible with large evanescent field for sensing applications. Optical wave guiding properties of such devices are discussed with numerical simulations. A dispersion as high as $-1000\ \mathrm{ps\,km^{-1}\,nm^{-1}}$ is obtained by reducing the radius of the OFM. The ZDW can be flexibly designed in the range of 600 nm to 2 μm by choosing the proper OFM radius from 500 nm to 2.5 μm. The sensitivity of a Bragg grating based OFM is also calculated. It can reach 1100 nm/RIU because of the large outside evanescent field. We believe that the OFM devices will have important applications in optical communication, nonlinear optics and fiber sensing.

Acknowledgements This work in supported by the National 973 program of China under Contract Nos. 2010CB327803 and 2006CB921805 and the China NSFC program under Contract Nos. 60977039 and 10874080. The authors also acknowledge the support from the New Century Excellent Talents program and the Changjiang scholars program.

References

1. C.A. Millar, B.J. Ainslie, M.C. Brierley, S.P. Craig, Electron. Lett. **22**, 322 (1986)
2. M.S. Dinleyici, D.B. Patterson, J. Lightwave Technol. **15**, 2316 (1997)
3. M.H. Chiu, S.F. Wang, R.S. Chang, Opt. Lett. **30**, 233 (2005)
4. G. Brambilla, V. Finazzi, D.J. Richardson, Opt. Express **12** (2004)
5. T. Limin, R.R. Gattass, J.B. Ashcom, H. Sailing, L. Jingyi, S. Mengyan, I. Maxwell, E. Mazur, Nature **426**, 816 (2003)
6. M. Sumetsky, Y. Dulashko, A. Hale, Opt. Express **12**, 3521 (2004)
7. X.S. Jiang, L.M. Tong, G. Vienne, X. Guo, A. Tsao, Q. Yang, D.R. Yang, Appl. Phys. Lett. **88**, 223501 (2006)
8. F. Xu, V. Pruneri, V. Finazzi, G. Brambilla, Opt. Express **16**, 1062 (2008)
9. F. Xu, P. Horak, G. Brambilla, Opt. Express **15**, 9385 (2007)
10. F. Xu, G. Brambilla, Appl. Phys. Lett. **92**, 101126 (2008)
11. J.-l. Kou, J. Feng, Q.-j. Wang, F. Xu, Y.-q. Lu, Opt. Lett. **35**, 2308 (2010)
12. J. -l. Kou, J. Feng, L. Ye, F. Xu, Y. -q. Lu, Opt. Express **18**, 14245
13. G. Brambilla, F. Xu, P. Horak, Y. Jung, F. Koizumi, N.P. Sessions, E. Koukharenko, X. Feng, G.S. Murugan, J.S. Wilkinson, D.J. Richardson, Adv. Opt. Photon **1**, 107 (2009)
14. A.W. Snyder, J.D. Love, *Optical Waveguide Theory* (Chapman & Hall, London, 1983)
15. K. Okamoto, *Fundamentals of Optical Waveguides*, 2nd edn. (Academic Press, San Diego, 2007)
16. A. Yariv, P. Yeh, *Optical Electronics in Modern Communications*, 6th edn. (Oxford University Press, London, 2006)
17. G.P. Agrawal, *Fiber-Optic Communications Systems*, 3rd edn. (Wiley, New York, 2002)
18. D.A. Akimov, A.A. Ivanov, M.V. Alfimov, S.N. Bagayev, T.A. Birks, W.J. Wadsworth, P.S. Russell, A.B. Fedotov, V.S. Pivtsov, A.A. Podshivalov, A.M. Zheltikov, Appl. Phys. B **74**, 307 (2002)
19. G. Brambilla, F. Koizumi, V. Finazzi, D.J. Richardson, Electron. Lett. **41**, 795 (2005)
20. W.J. Wadsworth, A. Ortigosa-Blanch, J.C. Knight, T.A. Birks, T.P.M. Man, P.S. Russell, J. Opt. Soc. Am. B **19**, 2148 (2002)
21. K. Shi, F.G. Omenetto, L. Zhiwen, Opt. Express **14** (2006)
22. P. Falk, M.H. Frosz, O. Bang, Opt. Express **13** (2005)
23. V. Hodzic, J. Orloff, C.C. Davis, J. Lightwave Technol. **22**, 1610 (2004)
24. W. Ding, S.R. Andrews, S.A. Maier, Opt. Lett. **32**, 2499 (2007)
25. X. Fang, C.R. Liao, D.N. Wang, Opt. Lett. **35**, 1007
26. D. Grobnic, S.J. Mihailov, H.M. Ding, C.W. Smelser, IEEE Photon. Technol. Lett. **18**, 160 (2006)
27. C. Hong-Wei, T. Chuen-Lin, L. Wen Fung, L. Shane-Wen, in *2007 IEEE/LEOS Int. Conf. Optical MEMS and Nanophotonics*, pp. 119–120
28. K. Schroeder, W. Ecke, R. Mueller, R. Willsch, A. Andreev, Measur. Sci. Technol. **12**, 757 (2001)
29. F. Xu, G. Brambilla, Y. Lu, Opt. Express **17**, 20866 (2009)
30. A.N. Chrysis, S.M. Lee, M. Dagenais, in *2004 IEEE LEOS Annu. Meet. Conf. Proc.* (IEEE Cat. No. 04CH37581), vols. 431–432, vols. 434–435 (1010) (2004)